Design of 30-T pulsed magnetic field generator for magnetized high-energy-density plasma experiments

R. V. Shapovalov,[1,2,*] G. Brent,[2] R. Moshier,[2] M. Shoup,[2] R. B. Spielman,[2] and P.-A. Gourdain[1,2]

[1]*Department of Physics and Astronomy, University of Rochester, Rochester, New York 14627, USA*
[2]*Laboratory for Laser Energetics, University of Rochester, Rochester, New York 14623, USA*

This paper presents the conceptual design of a high-voltage pulser intended to generate 30-T magnetic fields for magneto-inertial fusion experiments at the OMEGA facility. The pulser uses a custom capacitor bank and two externally triggered spark gaps to drive a multiturn coil. This new high-voltage pulser is capable of storing 10 times more energy than the previous system, using a higher charge voltage (from 20 to 30 kV) and a larger capacitance (from 1 to 5 μF). Circuit simulations show that this pulser can deliver 100 kA into a 60-nH, 14-mΩ coil with a rise time of 1 μs. For a coil with two turns with an average coil diameter of 7.8 mm, this current translates into a 32-T peak magnetic field at coil center. This is a factor of 3 increase in the peak magnetic field compared to the present generator magnetic field capabilities.

I. INTRODUCTION

Magnetized plasmas and magnetized, inertial-confinement-fusion (ICF) experiments are an important milestone in fusion energy research. Pioneered on the OMEGA laser [1], this research integrates basic plasma physics, transport in magnetized plasmas, alpha-particle energy deposition in ICF capsules, and magneto-inertial-fusion concepts [2–6]. It also enables scientists to tackle more fundamental physics questions by studying positron focusing [7], astrophysical shocks [8–10], magnetized plasma jets, and magnetic reconnection [11]. At the OMEGA laser facility, a high-magnetic field is generated using the magneto-inertial fusion electrical discharge system (MIFEDS). The MIFEDS is a discharge pulser optimized to generate a high-current pulse into a magnetic coil. The pulser is installed inside the ten-inch-manipulator (TIM) unit and coil is positioned inside the OMEGA target chamber by moving the MIFEDS's TIM unit to the appropriate location. Unfortunately, the TIM constraints (volume and weight) fundamentally limit the energy that is available for the production of magnetic fields and the upgrade of the MIFEDS system is urgently needed.

MIFEDS-2 is a second-generation, high-voltage pulser/coil system currently used for magnetized, high-energy plasma experiments at the OMEGA and OMEGA-EP laser facilities [12]. The present system combines two, 500-nF (General Atomics) capacitors followed by a single spark gap (Excelitas GP-14B) switch, conical, coaxial transmission line and magnetic coil. The pulser total internal inductance is measured to be 139 nH and the pulser internal resistance is about 130 mΩ. The capacitors can be charged up to 20 kV which corresponds up to 200 J of initial pulser energy. Even for a low-inductance coil, these driver values limit the current to about 40 kA, making it difficult to reach a magnetic field larger than 20 T.

In this paper, we present the design of MIFEDS-3, a new high-voltage pulser capable of generating magnetic fields greater than 30 T. The general view of the MIFEDS-3 pulser is shown in Fig. 1. The pulser is comprised of two, custom General Atomics 2.5-μF capacitors connected in parallel and charged to a maximum voltage of 30 kV. At this charging voltage, the stored capacitor energy is 2.25 kJ, which is 10 times larger than the energy available in the MIFEDS-2 system. This gain in energy is achieved by increasing the physical size of the capacitors, requiring the HV power supply to be moved outside of the OMEGA TIM. Each of the two pulser capacitors are each discharged through a single, triggered spark gap (Excelitas GP-14B). The estimated internal pulser inductance is 90 nH, and the internal series resistance is less than or equal to 140 mΩ. We believe that MIFEDS-3 gives the best magnetic-field performance possible on OMEGA given the volume and weight limitations imposed on the pulser by the TIM. MIFEDS-3, similar to MIFEDS-2, uses bubble-style packaging (the pulser is installed inside an air bubble unit, which is placed inside the TIM under vacuum) and all vacuum-air interfaces were designed with the same specifications as the MIFEDS-2 system. Because MIFEDS-3 will be charged to a voltage higher than MIFEDS-2, 30-kV
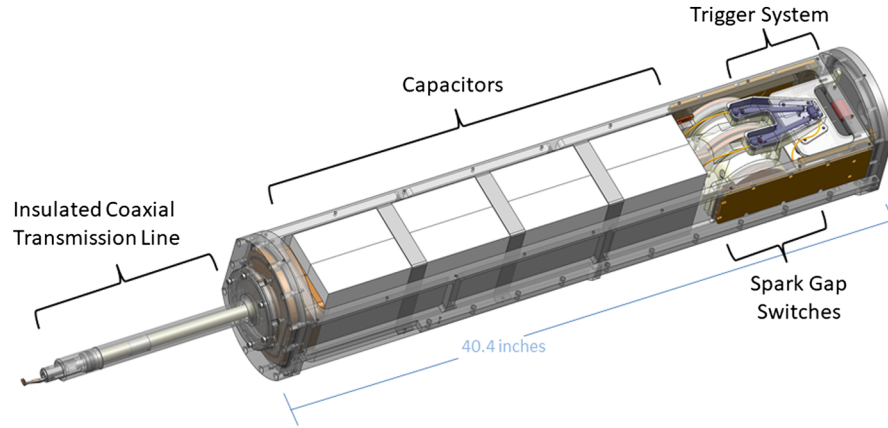
*rshapova@ur.rochester.edu

FIG. 1.   MIFEDS-III design view.

voltage, to prevent any possible voltage breakdown, a plastic sleeve is inserted inside the MIFEDS-3 coaxial transmission line. We anticipate significant improvements in MIFEDS-3 performance as compared to the present MIFEDS-2 pulser.

We first present the detailed MIFEDS-3 pulser circuit simulations into a typical 60-nH, 14-mΩ coil. We next discuss how the driver parameters scale with the coil inductance. Finally, we present the magnetic field calculations for 1-, 2-, 3-, and 4-turn coils and compare them with the MIFEDS-2 pulser. The MIFEDS-3 pulser is capable of suppling a maximum current of 100 kA. We expect that the MIFEDS-3 pulser will generate more than 30-T peak magnetic field inside the simple, 2-turn magnetic coil.

As will be shown in a following section, for low-inductance coils below 400 nH, the expected time to peak of the current is less than 2 μs and we do not expect the coil motion to significantly affect its magnetic field. Though we do not include an extended calculation of the coil's motion, heating and the physics of the skin depth on the surface of the coil, our simulations give us a solid understanding of what can be expected from the proposed MIFEDS-3 pulser and how its performance is compared to the presently in use MIFEDS-3 pulser. The comparisons of MIFEDS-3 with other compact high-magnetic field generators [13,14,15] for laser-plasma experiments is briefly discussed at the end.

II. PULSER CIRCUIT MODELING

We first present detailed circuit simulations into a typical MIFEDS coil. For consistency, we assume a 2-turn coil with average coil diameter of 7.8 mm that is made of 24-AWG (American wire gauge) copper-insulated wire. The 24-AWG wire has an outer diameter of 762 μm (including insulation) and a copper core diameter of 508 μm. For a single turn, the coil inductance can be approximated by [16] $L \approx \mu_0 R[\ln(8R/r) - 1.75]$, where μ_0 is the vacuum permeability, R is the coil radius, and r is the wire radius. The total coil resistance was simply calculated as $R = \rho l/S$, where ρ is wire resistivity at room

temperature, and r and S are the wire radius and cross-section area, correspondingly. Some discussions on why this simple formula should not affect much the driver performance will be made later. The total wire length equals to $l = N\pi d + 12$ cm, where N is the number of turns, d is the coil diameter, and 12 cm is an extra length of the coil wire legs. For $N = 2$ turn coil, the coil inductance is 60 nH (N^2 times larger), the total wire length is 17 cm, and the coil resistance is 14 mΩ.

A. Simulations of pulser parameters into the matched 60-nH, 14-mΩ coil

In the following simulations, we follow the "matched" load approach, $R = \sqrt{L/C}$. This is an ideal case for the high-current driver when one wants simultaneously to maximize the load current and minimize the voltage reversal (i.e., ringing) inside the system [17]. This case should not be confused with the so-called "critically matched" load case $R = 2\sqrt{L/C}$, which also is very important for pulsed-power applications, but in general delivers slightly less current as compared to the matched load case. The total pulser inductance (internal value plus coil value) is equal to 150 nH, and the total pulser resistance is matched to $\sqrt{L/C}$ and equals 170 mΩ. The matched value is slightly larger than the total pulser resistance (internal value plus coil value) of 154 mΩ and can be compensated by installing in-series high-resistance wire, if desired. It is important to note that the MIFEDS-3 internal resistance, 140 mΩ is, by design, close to the matched $\sqrt{L/C}$ pulser value, 170 mΩ, maximizing the load peak current and preventing the unwanted late-time current oscillations. We assume, for simplicity, no change in the wire resistance during the current pulse. This should be a good assumption, as the coil resistance is a small portion of the total pulser resistance. The total wire resistance for $N = 2$ turn coil is 14 mΩ which accounts for only 10% compared to the MIFEDS-3 internal inductance. In this case, the increase in the coil resistance due to the coil
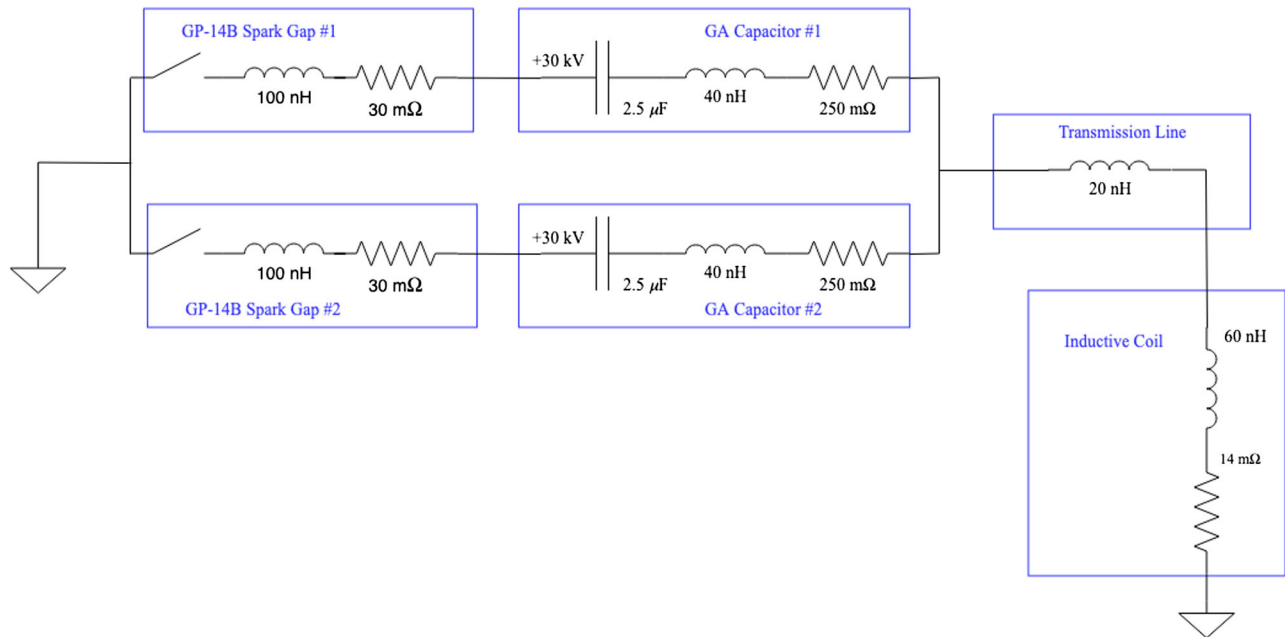
FIG. 2.   MIFEDS-III circuit diagram.

heating and plasma development should not affect much the total driver performance. All simulations are performed with the SCREAMER [18,19], a special-purpose pulsed-power circuit simulations tool.

The MIFEDS-3 pulser circuit diagram is shown in Fig. 2. Each of the two, 2.5-μF GA capacitors is charged to 30 kV and each is triggered through a single, triggered spark gap GP-14B. The inductance of each capacitor is about 40 nH and its equivalent series resistance is about 30 mΩ. The inductance of the switch is about 100 nH and its resistance is about 250 nH. The inductance of the transmission line is estimated to be around 20 nH which bridged with 60-nH, 14-mΩ 2-turn coil described above. Though, the total pulser internal inductance can be estimated to be equal to $(100 \text{ nH} + 40 \text{ nH})/2 + 20 \text{ nH} = 90 \text{ nH}$, and the total internal resistance is about $(30 \text{m}\Omega + 250 \text{m}\Omega)/2 = 140 \text{m}\Omega$.

The simulations of the current and voltage waveforms are presented in Fig. 3. A peak current of 95 kA is reached 1.05 μs after the start of the current waveform (the quarter-cycle time). The maximum coil voltage is 12 kV at the beginning of the coil pulse, and the minimum voltage is -2.8 kV at about 2.4 μs after the pulse starts. The resistive part of the voltage drop, thin dashed line, reaches its maximum value of 1.9 kV at 1.05 μs, and the inductive part of the voltage, thin dot-dashed line, follows closely the total voltage applied to the coil. We observe that both the positive and the negative peak currents are well inside the capacitor's safety margins. The negative reversal current is -16 kA at a time of ~ 4 μs with minimal current oscillations afterward. The presented pulser design, being very close to the matched load circuit, optimizes the coil peak current but limits the pulser current oscillations at later times.

It is interesting to compare the stored electrical energy of the pulser with the electrical energy delivered to the coil at the time of peak current, 1.05 μs. The total energy stored in the pulser is 2.25 kJ. The total energy delivered to a 60-nH coil, including its resistive and inductive parts, is plotted in Fig. 4. The peak energy delivered to the coil is ~ 400 J or $\sim 18\%$ of the initial energy stored in the capacitor. The resistive energy heats the coil and by the time of the current peak only $42\% (\sim 110 \text{ J}/ \sim 260 \text{ J})$ of the total resistive contribution is deposited in the coil. The inductive part of the energy, as expected, reaches its maximum value of about 270 J at the time of the peak current. The MIFEDS-3 pulser delivers 12% of the initially
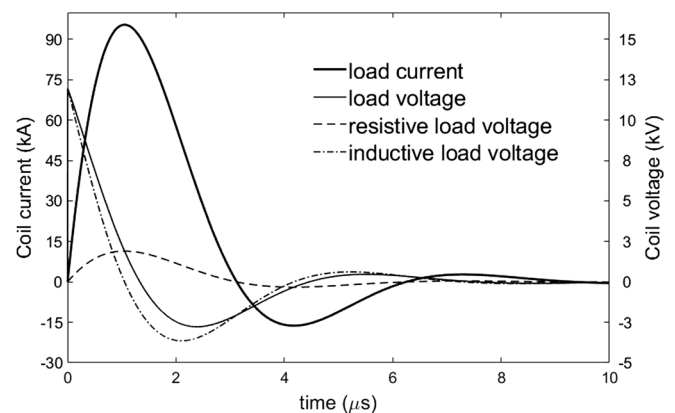

FIG. 3.   Simulations of the current and voltage waveforms into a matched 60-nH coil are shown. The thick solid line is the total load current, the thin solid line is the load total load voltage, the dashed line is the load resistive voltage, and the dot-dashed line is the load inductive voltage.
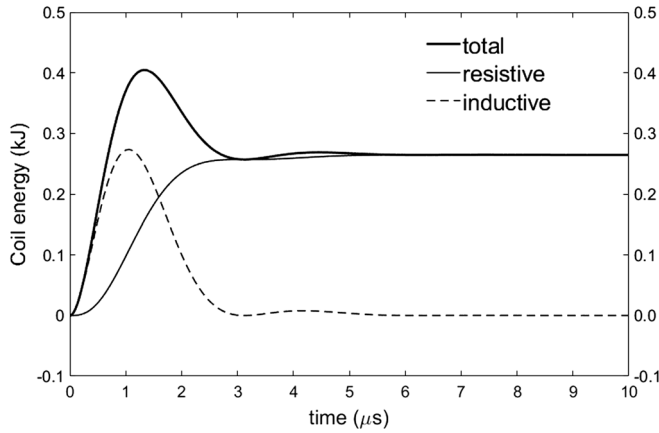
FIG. 4.   The energy deposition calculations into a matched 60-nH coil. The thick solid line is the total energy delivered to the coil, the thin solid line is its resistive part, and the thin dotted line is its inductive part.
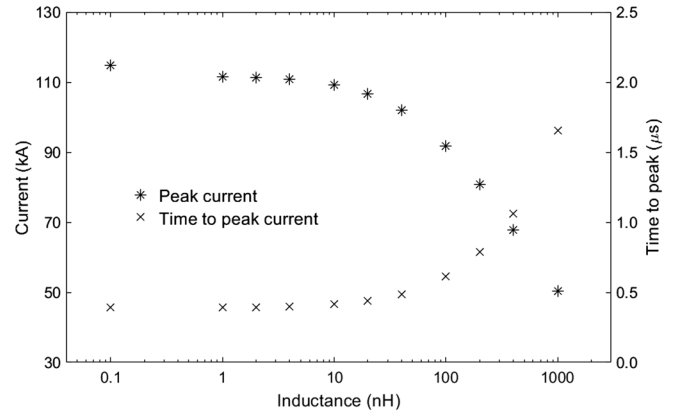

FIG. 5.   MIFEDS-3 coil peak current (asterisk) and time-to-peak current (times) calculations as a function of coil inductance. The coil resistance is assumed to be 20 mΩ for all cases.

stored electrical energy into the magnetic energy of this 60-nH coil. It is tempting to increase the time to peak of the current (larger capacitors) to increase the total energy stored inside the magnetic field, but longer current rise times will result in increased motion (expansion) of the coil wires, preventing the coil from reaching its maximum value of peak magnetic field. Keeping this current rise below 1–2 μs gives an optimal coupling between the initial stored energy and the magnetic energy. Current rise times shorter than 1-μs result in excessive coil voltages when the peak current is increased beyond MIFEDS-2 currents.

B. Scaling of the pulser's parameters with the coil inductance

Other experiments may require different coils and we are interested in the dependence of the pulser output parameters on coil inductance. The most important pulser parameters affecting the resulting coil magnetic field are the pulser peak current and the time-to-peak current. A scan of these pulser parameters as a function of coil inductance is presented in Fig. 5. Each data point is a separate SCREAMER run with the coil inductance value from the horizontal axis. The total driver inductance is, as before, the sum of the pulser internal inductance plus the inductance of the corresponding coil. However, we do not assume the matched, $\sqrt{L/C}$, resistance value as we did earlier for 2-turn, 60-nH coil. Instead, we assume the constant coil resistance of 20 mΩ, and the constant total pulser resistance of 160 mΩ (140 mΩ + 20 mΩ) for all SCREAMER runs for all pulser coils. A more accurate estimate of the coil resistance will be possible when the coil wire length is better known.

As expected, the pulser peak currents and time-to-peak currents are monotonic functions of the coil inductance. As we increase the coil inductance from 100 pH to 100 nH, the peak currents decrease from 115 kA down to 50 kA,

and time-to-peak currents increase from 800 ns up to 3.3 μs. For low-inductance coils below 40 nH, the peak currents are slightly above the operational pulser limit of 100 kA (switch and capacitor limited). For the high-inductance coils above 400 nH, the time-to-peak currents become larger than 2 μs, and the coil performance will degrade because of the increased wire motion. These calculations suggest that the optimal pulser performance is achieved when the coil inductance is in the range of 40 to 400 nH.

III. CALCULATION OF COIL MAGNETIC FIELD

Once the coil geometry is established and the coil current is simulated, the coil magnetic field can be calculated. This task is not trivial and usually requires numerical simulations. However, for the simple coil geometries, and if the coil shape is preserved on the time scale of the peak current, the coil magnetic field can be approximated with a simple formula. That is a good assumption for coils with inductance below 400 nH, because, as was already discussed, the time-to-peak current for such coils is below 2 μs, and the coil movement can be neglected. In the case of N-turn coil, the peak magnetic field at the coil center can be approximated by $B_0 = \mu_0 N I / d$, where I is the coil current, N is the number of the coil turns, and d is the coil diameter. In this case, the magnetic field waveform, $B(t)$, is simply the scaled function of the current waveform, $I(t)$, which can be readily calculated with SCREAMER, or any other circuit code.

A. Estimations of the magnetic field into a simple, 2-turn, 60-nH coil

Here we aim to calculate the magnetic field generated inside a typical coil and compare the coil performance with the present, MIFEDS-2, pulser. The most direct approach to compare MIFEDS-2 and MIFEDS-3 pulsers is without the matched load, $\sqrt{L/C}$, assumption. In this case, the
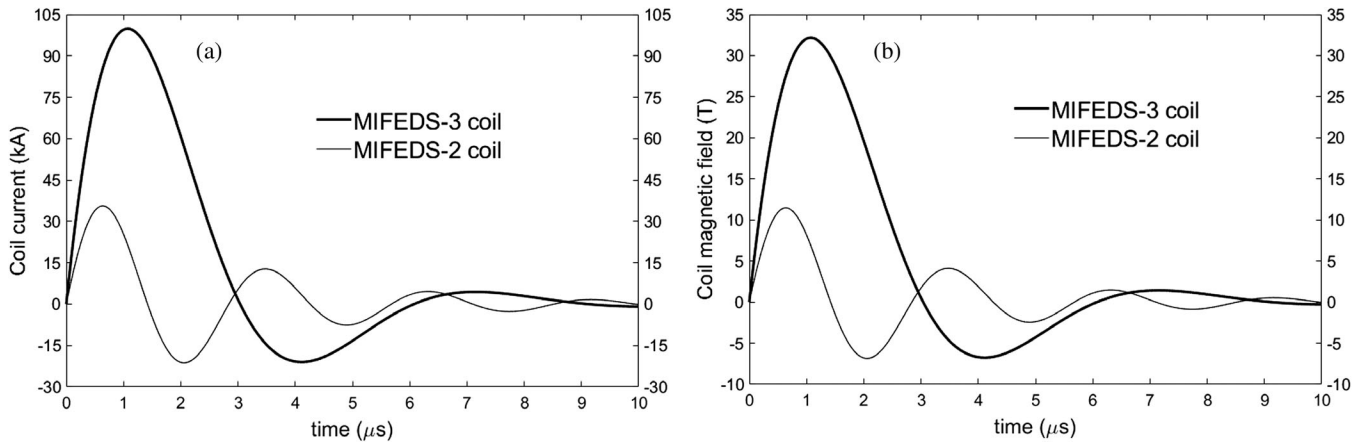
FIG. 6.   Simulations of the currents and magnetic field waveforms into the 60-nH, 14-mΩ coil. Part (a) corresponds to the MIFEDS coil current and (b) shows the peak magnetic field in the coil.

pulser total resistance is a sum of its internal value (130 mΩ for MIFEDS-2, and 140 mΩ for MIFEDS-3) and the resistance of the coil. Once again, we consider a simple, 2-turn coil with average coil diameter of 7.8 mm made of 24-AWG copper insulated wire. The inductance and resistance of this coil was calculated to be 60-nH and 140 mΩ, respectively. The rest of the pulser parameters are as discussed in the Introduction.

Both the current and magnetic field calculations into a 2-turn, 7.8-mm diameter coil are presented, Fig. 6. As can be seen, for the new MIFEDS-3 pulser, the simulations predict maximum 100-kA peak current at about 1.1 μs. Not a surprise, this is a factor of 3 larger than MIFEDS-2 current. It is interesting to observe that the MIFEDS-3 current waveform is very close to the matched load case presented in Fig. 3. The slight difference in the peak and time-to-peak values accounts for the driver resistance mismatch as compared to the matched load. The coil magnetic fields [Fig. 6(b)] are simply the scaled waveforms of the coil currents. The peak magnetic field generated inside the MIFEDS-3 coil reaches 32 T by the time of the current peak (1.1 μs), which is, as expected, the factor of 3 larger as compared to the present MIFEDS-2 pulser.

The FWHM for MIFEDS-3 current and magnetic field waveforms is about twice as large as the MIFEDS-2 driver. In magnetized, high-energy-density experiments on OMEGA, the lasers are triggered at the current peak [12], a time interval where the current change is limited to ±5% (also called the flattop window). The flattop window is about 770 ns, relaxing the allowable jitter in triggering MIFEDS-3, compared to MIFEDS 2, which has a 380-ns window.

B. Dependence of the coil magnetic field on the total number of turns

In experiments calling for a stronger magnetic field, it is possible to increase the total number of turns in the coil, keeping the coil inductance the same by reducing the coil

diameter. It is also possible to increase the coil magnetic field keeping the coil diameter the same but increasing the total number of turns. Both cases are equally possible and result in the larger coil magnetic field. However, in the first case, the resulting magnetic field is concentrated over a small coil volume, and in the former case, the magnetic field is applied to the larger coil volume.

Here, we consider the generation of higher magnetic fields using four different coils, all having the same coil diameter, but with 1, 2, 3, and 4 total number of turns. To be consistent with our previous simulations, we assume all coils made of the same 24-AWG copper-insulated wire with 7.8-mm average coil diameter. The inductance and resistance of these coils are calculated utilizing the same approach used for the 2-turn coil. The coil inductances are 15, 60, 135, and 240 nH with resistances of 12, 14, 16, and 18 mΩ, for coils having 1, 2, 3, and 4 turns, respectively. Using SCREAMER, we simulate the current $I(t)$ waveform, and, later, using the formula for magnetic field $B_0 = \mu_0 NI/d$, calculate the resulting coil magnetic field, $B(t)$. The current waveform simulations for coils with a different number of turns are presented in Fig. 7(a) and the corresponding magnetic field waveforms are plotted in Fig. 7(b).

It is not obvious that an increase in the total number of turns, N, will result in a larger magnetic field. Indeed, as we increase the total number of turns, the coil inductance increases, and the coil peak current, $I(t)$, decreases. Because the magnetic field, $B(t)$, is proportional both to $I(t)$ and N, the resulting magnetic field is not obvious. As can be seen from Fig. 7, left plot, the peak current gradually decreases as we increase the coil inductance. There is as much as 110-kA peak current with a 1-turn, 15-nH coil. The current decreases to about 80 kA for 4-turn, 240-nH coil. The peak magnetic fields monotonically increase as we increase the total number of turns. The peak magnetic fields are 18, 32, 42, and 50 T for the coils having 1, 2, 3, and 4 turns, correspondingly. It appears that the coil current, $I(t)$, is a weaker function than the total number
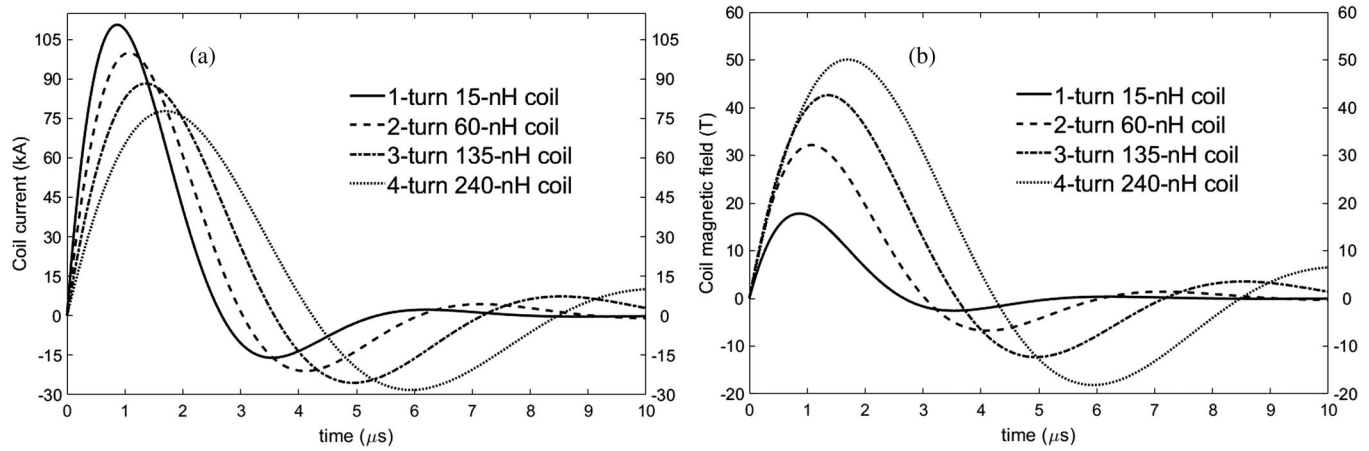
FIG. 7.   MIFEDS-3 simulations into 1-, 2-, 3- and 4-turn coils. All coils have the same 7.8-mm average coil diameter. The left plot shows the SCREAMER current waveform simulations, and the right plot shows the corresponding coil magnetic field waveforms.

of turns, N, and the resulting magnetic field becomes larger as we increase the coil number of turns.

It should be also noted that, as we increase the number of turns, the time-to-peak current increases as well. It appears that 1–4-turns are the optimal number of coil windings for the case with 7.8-mm average coil diameter. A larger number of turns will increase the time-to-peak current above 2 μs, which will result in motion of the coil wires during the pulse and a degradation of the peak magnetic field.

C. Comparison of MIFEDS-3 with MIFEDS-2 pulser and other compact high-magnetic field generators

The comparison of the calculated peak magnetic fields for the proposed new MIFEDS-3 pulser and presently in operation MIFEDS-2 system is presented in Fig. 8. We assume 1-turn, 2-turn, 3-turn, and 4-turn coils having inductances of 15, 60, 135, and 240 nH, respectively, both for MIFEDS-3 and MIFEDS-2 pulsers calculated as
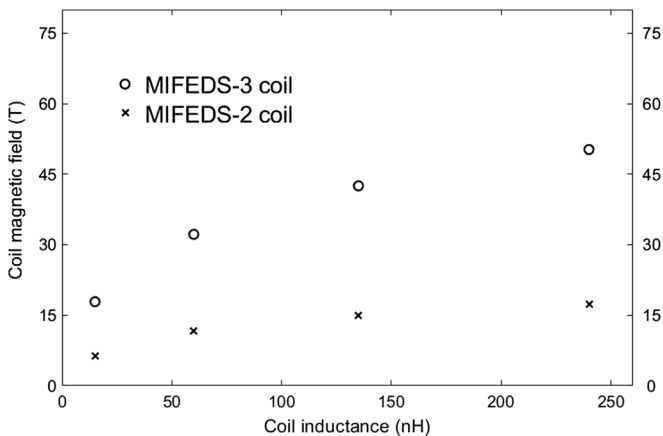

FIG. 8.   Calculations of peak magnetic fields are plotted as a function of coil inductance. All coils have the same average coil diameter of 7.8 mm. The coil inductances are 15, 60, 135, and 240 nH for 1-turn, 2-turn, 3-turn, and 4-turn coils, respectively.

described in the previous section. The peak magnetic fields for the new MIFEDS-3 pulser are from Fig. 7, right plot. The pulser internal circuit parameters, both for MIFEDS-2 and MIFEDS-3 systems, were discussed throughout the text and, for clarity, are summarized here. The internal inductance, resistance, and total capacitance are 1 μF, 139 nH, and 130 mΩ for MIFEDS-2 pulser, and 5 μF, 90 nH, and 140 mΩ for MIFEDS-3 pulser, correspondingly. The MIFEDS-2 was initially charged 20 kV, and MIFEDS-3 to 30 kV. As can be seen, the peak magnetic fields generated with the new pulser are the factor of 3 larger than peak magnetic fields generated inside the present MIFEDS-2 system. The increase in the peak magnetic fields is directly related to the capabilities of the upgraded pulser to supply the larger currents into the predefined magnetic coil. Also, the saturation of the peak magnetic fields can be seen as a function of the coil inductances—coil number of turns. For this coil with 7.8-mm diameter it is not practical to go to a higher magnetic field by increasing the number of coil's turn above 4. In addition to the saturation effect, the time-to-peak current exceeds 2 μs and the peak magnetic fields can degrade because of the increased coil motion.

The results presented in this paper can be scaled for different coil diameters and, in this way, the driver performance can be compared with some other compact high-magnetic field generators for laser-plasma experiments. The coil magnetic field is, both, proportional to the coil current, and inversely proportional to the coil diameter, as given by $B_0 = \mu_0 NI/d$. But the coil current is only a weak function of the coil diameter, and, in the first order, the coil magnetic field can be scaled as the inverse of the coil diameter. For the single-turn coil, the scaling relation can be written as $B_1/B_2 \sim d_2/d_1$. For example, our simulations predict that 7.8-mm diameter single-turn coil can generate 18-T peak magnetic field at the coil center (Fig. 7 or Fig. 8). Using the scaling relation just discussed above, we can estimate that about 14 T peak magnetic field is expected for 1-cm diameter, single-turn coil assuming no

change in the peak current. That is close to 13.9 T peak magnetic field when more careful analysis, taking into the account the current simulations, is performed.

Finally, we briefly discuss how the MIFEDS-3 performance is compared to some other high-magnetic field generators for laser plasma experiments [13–15], such as, two-capacitor and ten-capacitor pulsers currently in operation at the Texas Petawatt and the Z-Beamlet laser facilities. Both pulsers are portable, have a relatively small footprint, and can be moved back and forth [13] between Texas Petawatt and Z-Beamlet for the magnetized laser plasma experiments. The Sandia two-capacitor high-magnetic field pulser [15] is comprised of two capacitor-switch blocks each connected by six coaxial cables to the triplate transmission line leading to the magnetic coil inside the vacuum chamber. It has a total capacitance of 6.2-μF and system inductance of about 150 nH, which are very close to the MIFEDS-3 parameters (5-μF capacitance and 90-nH internal inductance). However, the Sandia two-capacitor system can be charged to larger 100 kV voltage as compared to maximum 30 kV for MIFEDS-3 pulsers. This higher charging voltage drives the higher peak current, which, in turn, results in the higher magnetic field coil's performance. When charged to the maximum 100 kV voltage, the two-capacitor pulser can deliver as much as 500-kA peak current with about 1.5-μs time to peak, which is factor of 5 larger than what is expected from the MIFEDS-3 pulser. According to $B_0 = \mu_0 N I / d$, for 1-cm diameter, single-turn coil, this peak current translates into 60-T peak magnetic field assuming no coil motion and other effects degrade the coil magnetic field performance.

The ten-capacitor pulser [15] is a larger counterpart of the two-capacitors system with similar design but ten capacitor-switch blocks arranged around the vacuum chamber instead of two. The pulser is intended to deliver 2-MA peak current and generate up to 200 T peak axial magnetic field into the single-turn, low-inductance coil. The testing reveals just above 1-MA peak current with 1.7-μs time to peak into single-turn, 5-nH coil when the pulser was half charged to 50 kV. The peak magnetic field for this coil was estimated to be over 100 T.

Of course, the higher magnetic field capabilities of the Sandia two-capacitor and ten-capacitors systems (60 T and 200 T versus 14 T for MIFEDS-3 pulser for 1-cm single-turn coil) are a direct consequence of the fact that the Sandia pulser has higher initial stored energy, which results in a higher peak current and a larger peak magnetic field. Unfortunately, the volume available inside the TIM unit, where the MIFEDS-3 pulser is intended to be installed, does not give to us the capability to farther increase the stored energy. We believe that MIFEDS-3 pulser design presented in this paper gives the best magnetic-field performance possible on the OMEGA laser facility given the volume and the weight limitations imposed on the pulser by the TIM. We would need to move the capacitors outside of the TIM units to increase the available stored energy inside the MIFEDS-next-generation pulser to farther increase the peak magnetic field of the coil.

IV. CONCLUSION

We describe the electrical design of the new MIFEDS-3 pulser. By increasing the current capabilities by a factor of 3, the proposed system can achieve stronger magnetic fields, while staying within the weight and volume constraints of the TIM. The MIFEDS-3 design has a total stored electrical energy 10 times larger than its predecessor and should reach 100-kA peak current in less than 1 μs, into a 60-nH, 14-mΩ coil. Assuming a 2-turn coil geometry with an average coil diameter of 7.8 mm this peak current gives a peak magnetic field of 32 T at the center of the coil. Even larger magnetic fields can be achieved using coils with more turns.

[1] T. R. Boehly, D. L. Brown, R. S. Craxton, R. L. Keck, J. P. Knauer, J. H. Kelly, T. J. Kessler, S. A. Kumpan, S. J. Loucks, S. A. Letzring, F. J. Marshall, R. L. McCrory, S. F. B. Morse, W. SekaJ. M. Soures, and C. P. Verdon, Initial performance results of the OMEGA laser system, Opt. Commun. **133,** 495 (1997).

[2] O. V. Gotchev, P. Y. Chang, J. P. Knauer, D. D. Meyerhofer, O. Polomarov, J. Frenje, C. K. Li, M. J.-E. Manuel, R. D. Petrasso, J. R. Rygg, F. H. Séguin, and R. Betti, Laser-Driven Magnetic-Flux Compression in High-Energy-Density Plasmas, Phys. Rev. Lett. **103,** 215004 (2009).

[3] J. P. Knauer, O. V. Gotchev, P. Y. Chang, D. D. Meyerhofer, O. Polomarov, R. Betti, J. A. Frenje, C. K. Li, M. J.-E. Manuel, R. D. Petrasso, J. R. Rygg, and F. H. Séguin,

Compressing magnetic fields with high-energy lasers, Phys. Plasmas **17,** 056318 (2010).

[4] P. Y. Chang, G. Fiksel, M. Hohenberger, J. P. Knauer, R. Betti, F. J. Marshall, D. D. Meyerhofer, F. H. Seguin, and R. D. Petrasso, Fusion Yield Enhancement in Magnetized Laser-Driven Implosions, Phys. Rev. Lett. **107,** 035006 (2011).

[5] M. Hohenberger, P. Y. Chang, G. Fiksel, J. P. Knauer, R. Betti, F. J. Marshall, D. D. Meyerhofer, F. H. Seguin, and R. D. Petrasso, Inertial confinement fusion implosions with imposed magnetic field compression using the OMEGA Laser, Phys. Plasmas **19,** 056306 (2012).

[6] D. H. Barnak, J. R. Davies, R. Betti, M. J. Bonino, E. M. Campbell, V. Yu. Glebov, D. R. Harding, J. P. Knauer, S. P. Regan, A. B. Sefkow, A. J. Harvey-Thompson, K. J. Peterson, D. B. Sinars, S. A. Slutz, M. R. Weis, and P.-Y. Chang, Laser-driven magnetized liner inertial fusion on OMEGA, Phys. Plasmas **24,** 056310 (2017).

[7] H. Chen, G. Fiksel, D. Barnak, P. Y. Chang, R. F. Heeter, A. Link, and D. D. Meyerhofer, Magnetic collimation of relativistic positrons and electrons from high intensity laser–matter interactions, Phys. Plasmas **21,** 040703 (2014).

[8] A. S. Liao, S. Li, P. Hartigan, P. Graham, G. Fiksel, A. Frank, J. Foster, and C. Kuranz, Numerical simulation of an experimental analogue of a planetary magnetosphere, High Energy Density Phys. **17,** 38 (2015).

[9] D. B. Schaeffer, W. Fox, D. Haberberger, G. Fiksel, A. Bhattacharjee, D. H. Barnak, S. X. Hu, and K. Germaschewski, Generation and Evolution of High-Mach-Number Laser-Driven Magnetized Collisionless Shocks in the Laboratory, Phys. Rev. Lett. **119,** 025001 (2017).

[10] D. B. Schaeffer, W. Fox, D. Haberberger, G. Fiksel, A. Bhattacharjee, D. H. Barnak, S. X. Hu, K. Germaschewski, and R. K. Follett, High-Mach number, laser-driven magnetized collisionless shocks, Phys. Plasmas **24,** 122702 (2017).

[11] G. Fiksel, W. Fox, A. Bhattacharjee, D. H. Barnak, P. Y. Chang, K. Germaschewski, S. X. Hu, and P. M. Nilson,

Magnetic Reconnection between Colliding Magnetized Laser-Produced Plasma Plumes, Phys. Rev. Lett. **113,** 105003 (2014).

[12] G. Fiksel, A. Agliata, D. Barnak, G. Brent, P.-Y. Chang, L. Folnsbee, G. Gates, D. Hasset, D. Lonobile, J. Magoon, D. Mastrosimone, M. J. Shoup III, and R. Betti. Note: Experimental platform for magnetized high-energy-density plasma studies at the OMEGA laser facility, Rev. Sci. Instrum. **86,** 016105 (2015).

[13] N. J. Riley, S. M. Lewis, M. L. Wisher, M. W. Kimmel, K. W. Struve, J. L. Porter, R. D. Bengtson, and T. Ditmire, Improved experimental resolution of the Vishniac over-stability in scaled late-stage supernova remnants, High Energy Density Phys. **22,** 64 (2017).

[14] K. W. Struve, J. L. Porter, and D. C. Rovang, Megagauss Field Generation for High-Energy-Density Plasma Science Experiments, Sandia Report No. SAND2008-7015, 2008.

[15] K. W. Struve, J. W. Argo, R. D. Bengtson, D. I. Headley, J. W. Kellogg, S. M. Lewis, J. L. Porter, H. J. Quevedo, M. E. Savage, B. Stoltzfus, C. J. Waugh, and M. Wisher, LDRD Final Report on Confinement of Cluster Fusion Plasmas with Magnetic Fields, Sandia Report No. SAND2011-8500, 2011.

[16] F. W. Grover, *Inductance Calculations* (Dover Publications, Mineola, 2004).

[17] M. G. Mazarakis and R. B. Spielman, A compact, high-voltage E-beam pulser, in *Proceedings of the 12th IEEE International Pulsed Power Conference, Monterey, CA* (IEEE, Piscataway, NJ, 1999), https://doi.org/10.1109/PPC.1999.825498.

[18] M. L. Kiefer and M. M. Widner, Screamer—a single-line pulsed-power design tool, in *5th IEEE Pulsed Power Conference, Washington, DC* (IEEE, Piscataway, NJ, 1985).

[19] R. B. Spielman and Y. Gryazin, *Screamer v4.0—a powerful circuit analysis code*, in *2015 IEEE Pulsed Power Conference, Austin, TX* (IEEE, Piscataway, NJ, 2015), https://doi.org/10.1109/PPC.2015.7296979.